Separation of disaccharide epimers, anomers and connectivity isomers by high resolution differential ion mobility mass spectrometry

Jordan Mastellone[#], K. M. Mohibul Kabir[#], Xiaojing Huang, and William A. Donald*

School of Chemistry, University of New South Wales, Sydney, NSW 2052, Australia.

[#]JM and KMMK contributed equally

*To whom correspondence should be addressed: w.donald@unsw.edu.au

Abstract

Glycans are ubiquitous, structurally diverse molecules that have specific and general roles involving metabolism, structure, and cell-to-cell signalling. Functional specificity depends strongly on the complexity of structures that polysaccharides can adopt based on their subunit composition, length, extent of branching, glycosidic bond connectivity and anomeric configuration. However, a rapid and comprehensive characterization of glycan isomers can be challenging owing to limitations associated with their separation. Here, ten composition, anomeric and connectivity disaccharide isomers were separated and detected using high-resolution differential ion mobility-mass spectrometry (DMS-MS, also known as FAIMS). Focus was primarily directed to compositional isomers corresponding to epimers that differ by the axial or equatorial position of a single hydroxyl group. DMS resolving power was enhanced 14-fold primarily by increasing the fraction of helium in the ion carrier gas and lowering the flow rate. At relatively high disaccharide concentrations, DMS-MS of each disaccharide resulted in complex and unique multi-peak spectra with up to ten fully and partially resolved peaks for β-1,4-mannobiose (Man-1,4β-Man), which can be attributed to the DMS separation and subsequent dissociation of ionic non-covalently bound oligomers into monomer ions. Each DMS spectrum has at least one differentiating peak that is not in the other spectra, indicating that DMS can be used to fully or partially resolve composition, configuration and connectivity isomers. At relatively low disaccharide concentrations, disaccharide epimers can also be readily separated by DMS. The integration of high-resolution, ambient pressure DMS with complementary reduced-pressure ion mobility and MS-based glycomics and glycoproteomics workflows may be useful for improving the characterization of glycans and glycosylated biomolecules.

Introduction

Glycans are of crucial importance in biological systems.[1, 2] Most cells in nearly all organisms are adorned with glycans that can have key roles in cell signaling and cell-to-cell recognition. Glycans contribute both generally and specifically to virtually all biological pathways, which can affect distinct intracellular mechanisms and phenotypic differences that only manifest at the whole-organism level.[3] However, the chemical complexity of glycan structures is astounding owing to compositional isomerism of monosaccharide building blocks, branching, and the presence of stereocenters at glycosidic linkages.[4] Glycans consist of monosaccharides linked by glycosidic bonds and exhibit many types of isomerism. Of the 75 known naturally occurring monosaccharide building blocks, 62 are found within ten general classes in which each class has the same elemental composition (*composition isomers*).[5] For example, in the hexoses, there are eight naturally occurring monosaccharides with the same elemental composition ($C_6H_{12}O_6$). Each of these building blocks has an anomeric hemiacetal/acetal carbon which can adopt a discrete axial (α) or equatorial (β) stereoisomeric configuration (*configuration isomers*), which can each connect to several possible carbons on an adjacent monosaccharide (*connectivity isomers*). In addition, there may be more than one glycosidic bond extending from a subunit, resulting in branched isomers.[6] Even when limited to the nine common monosaccharides found in humans, over 15 million tetrasaccharides are possible.[7] Thus, carbohydrates are considered more challenging to characterize than peptides and oligonucleotides.

The method of choice for certifying the purity of synthesized glycans is nuclear magnetic resonance (NMR) spectroscopy, which can provide highly detailed structural information.[8] However, NMR typically requires milligram quantities of analyte, which can often exceed biologically relevant levels. The separation and detection of glycans at trace (femtomolar) levels is possible using fluorescent tagging in lectin- or antibody- binding assays,

which has been proven useful for the targeted testing of hypotheses regarding glycan function.[9, 10]

Mass spectrometry is an alternative method for glycan analysis where many different glycans can be detected rapidly and nearly simultaneously with high sensitivity in a single measurement.[11] Although single-stage MS fundamentally cannot distinguish glycan isomers of equal *m*/*z*, tandem mass spectrometry (MS^n) analysis can yield diagnostic fragment ions. Connectivity isomers can be distinguished by use of MS^n, either through several stages of collision-induced dissociation (CID)[12] or ultra-violet photodissociation (UVPD).[13] Infrared multiphoton dissociation (IRMPD) can result in fragment spectra largely equivalent to multistage or high energy CID,[14-17] while electron-capture dissociation (ECD) can result in additional structurally informative dissociation pathways such as cross-ring cleavages.[18, 19] In matrix-assisted laser desorption ionization (MALDI), metastable precursor ions can undergo post-source fragmentation followed by CID fragmentation (in a TOF/TOF system) to obtain sequence information including connectivity isomerism.[20-23] Nevertheless, differentiating constitutional and compositional isomer analysis by MS^n is difficult because the resulting fragment ions have the exact same mass. Although relative fragment ion abundances may provide information for identifying constitutional and compositional stereoisomers, unambiguous identification can be highly challenging by MS^n methods alone.

A range of methodologies have been used to separate glycans using liquid chromatography (LC) with normal phase (polar), reverse phase (non-polar), anionic exchange, and antibody columns.[24-27] Capillary electrophoresis integrated with ESI-MS can be used to separate α2,3- and α2,6- sialic acid connectivity isomers.[28] However, like many other methods, the baseline resolved separation of configuration and composition isomers is challenging. Although the effects of such isomers in ubiquitous and well-studied glycans can often be minor,

the influence of subtle isomeric differences in more unusual glycans can often be crucial and specific.[6, 29]

The separation of glycan isomers using ion mobility spectrometry (IMS)-based methods has attracted significant recent attention, particularly in the use of low-electric field-based methods (e.g. drift tube and travelling wave IMS) in which ions are rapidly separated primarily based on their mass, charge, and collision cross sections.[30-34] Toraño et al.[35] utilized drift tube IMS (DTIMS) to identify isomeric N-glycans based on their conformer distribution 'fingerprints'. The partial separation of disaccharides using travelling wave IMS (TWIMS), through derivatization using 1-phenyl-3-methyl-5-pyrazolone (PMP) was demonstrated by Yang et al.[36] Williamson et al[37] used cyclic TWIMS to investigate complex peak patterns, often associated with IMS-based oligosaccharide analysis. Ujma et al.[38] demonstrated that cyclic IMS could separate isomeric pentasaccharides. Recently, TWIMS has also been combined with cryogenic infrared spectroscopy to separate disaccharide isomers.[39] Furthermore, structures for lossless ion manipulation (SLIM)-based IMS-IMS has been integrated with cryogenic infrared spectroscopy to enable the separation of a range of disaccharides[40] and oligosaccharides[41].

A complementary ion-mobility based method to DTIMS and TWIMS is differential ion mobility spectrometry (DMS), also known as field asymmetric ion mobility spectrometry (FAIMS). In DMS, ion separation typically occurs at ambient pressure and by use of extremely high electric fields in which ion mobility depends non-linearly on the electric field and is less dependent on the mass, charge state and collision cross section of ions than in lower field ion mobility-based methods.[42-54] Thus, DMS and low-field IMS methods are complementary and their integration is making high performance tandem ion separations feasible. For DMS separation, ions are carried between two electrodes by a gas. An alternating current (AC), bisinusoidal, asymmetric electric potential is applied across the electrodes to radially disperse ions as they traverse through the channel between the electrodes. In the resulting asymmetric

field, the ions experience the high electric field for less time than that of the lower field portion of the AC waveform. Ions that have equal displacement in the high and low electric field segments are transmitted. A particular ion can be selectively transmitted by superimposing a compensation voltage (V_c) onto the asymmetric waveform corresponding to a compensation electric field (E_c), resulting in the effective filtering of ions. The use of planar DMS electrode geometries with relatively long channel lengths (6.5 cm) and high concentrations of low-molecular weight carrier gases has been demonstrated to have higher resolving power than alternative DMS methods. High resolution DMS can be used to separate peptide isomers that differ by the position of a single methyl group,[55] protein protonation isomers,[56] diastereomers,[57, 58] and isomeric glycopeptides.[59]

Here, high resolution DMS is demonstrated to be capable of differentiating disaccharide isomers, including composition, configuration and connectivity isomers. Disaccharides can be considered fundamental models to reduce the complexity of glycan structure into a single isomeric subunit, in which two glycosydically-linked monosaccharides can differ based on epimeric, anomeric and connectivity isomerism. Such isomerism applies to all glycans and thus, disaccharides are useful for evaluating the separation performance of different analytical platforms. An emphasis is placed on composition isomers because they have more closely related collision cross sections than configuration and connectivity isomers (owing to a conserved glycosidic bond structure) and have been more challenging to resolve by IMS and DMS.

Experimental and methods

Materials

4-O-α-D-glucopyranosyl-D-glucose (**1**, Glc-1,4α-Glc), 4-O-(α-D-galactopyranosyl)-D-glucose (**2**, Gal-1,4α-Glc), 4-O-β-D-glucopyranosyl-D-glucose (**3**, Glc-1,4β-Glc), 4-O-β-D-galactopyranosyl-D-glucose (**4**, Gal-1,4β-Glc), 3-O-(β-D-glucopyranosyl)-D-glucose (**5**, Glc-

1,3β-Glc), 3-O-(β-D-galactopyranosyl)-D-glucose (**6**, Gal-1,3β-Glc), 4-O-β-D-galactopyranosyl-D-mannose (**7**, Gal-1,4β-Man), 4-O-(β-D-glucopyranosyl)-D-mannose (**8**, Glc-1,4β-Man), 4-O-(β-D-Mannopyranosyl)-D-glucose (**9**, Man-1,4β-Glc), and 4-O-(β-D-mannopyranosyl)-D-mannose (**10**, Man-1,4β-Man) were obtained from commercial sources and used without further purification (see Table S1 for full details). Deionized water was obtained using a MilliQ water purification system (Merck, Darmstadt, Germany). Sodium chloride and HPLC-grade methanol were obtained from VWR (Radnor, PA, USA). High purity nitrogen and ultra-high purity helium gas cylinders (ALPHAGAZ™) were obtained from Air Liquide Australia Ltd. (Melbourne, VIC, Australia). Stock solutions were prepared by sonicating 1 mg of each disaccharide or sodium chloride in 1 mL of deionized water, and dilution in HPLC-grade methanol (90% v/v) and deionized water (10% v/v) to a final disaccharide concentration of either 1 mM with 1 mM sodium chloride for oligomer experiments, or to 20 uM disaccharide and 20 uM sodium chloride.

Differential ion mobility-mass spectrometry

All experiments were performed using a linear trap quadrupole MS (LTQ XL, Thermo Scientific, San Jose, CA, USA) integrated with a planar DMS (Heartland Mobility, Wichita, KS, USA). An electrodynamic ion funnel (Heartland Mobility, Wichita, KS, USA) was used as the interface between the DMS and the MS to increase ion transmission efficiencies. Liquid samples were infused by positive-mode ESI (+3.4 kV, 0.4 uL/min) through a borosilicate capillary emitter (76 μm inner diameter) via a syringe pump (NE-300 by New Era Pump Systems, Farmingdale, NY, USA). Mass spectra were obtained from 100 to 1000 *m*/*z* with 10 microscans and a maximum injection time of 20 μs. Ion transmission through the ion funnel was optimized to maximize ion signal (Table S2). In some specific cases, CID was performed using a 2 *m*/*z* isolation window centered on the ion of interest using helium collision gas at a normalized collision energy of 5% with 30 ms activation time.

The DMS instrument has two parallel, planar electrodes that are 65 mm long, 35 mm wide and separated by a 1.88 mm analytical gap. Ions generated by ESI are injected orthogonally into the gap through a cylindrical inlet (2 mm diameter) of a curtain plate (+1.0 kV) and a second cylindrical inlet (1 mm diameter) in one of the DMS electrodes. The carrier gas composition ranged from 100 to 50% nitrogen gas mixed with 0 to 50% helium, and the flow rate was controlled from 0 to 2 L/min using digital flow meters (MKS instruments, Andover, MA, USA). An in-house heater was used to apply up to 200 °C to the carrier gas tubing, consisting of ~2 m of brass tubing coiled to a diameter of 40 mm and wrapped by silicone rubber heating tape, which was powered by a digital controller via temperature feedback from a type-K thermocouple. Pre-scan heating was performed for 3 hours prior to measurements to thermally equilibrate the DMS electrodes by applying up to 150 °C to the carrier gas tubing with the RF waveform dispersion voltage set to 4.00 ± 0.01 or 4.20 ± 0.01 kV. Carrier gas temperature was indirectly sampled using a type-K thermocouple and a resistance temperature detector (RTD) probe by measuring the temperature at the carrier gas tubing outlet connected to a partially sealed polypropylene tube of 25 mm diameter and 100 mm length (Figure S1).

DMS-MS spectra were obtained from the raw MS files by smoothing across 15-scan intervals using Boxcar averaging in Xcalibur 2.2 QualBrowser (Thermo Fisher Scientific, San Jose, CA, USA). In the plotted spectra, shaded envelopes around median lines correspond to two standard deviations from the mean of 3-4 consecutive replicates. Figures were prepared using Origin Pro 2016b (OriginLab Corporation, Northampton, MA, USA).

Results and Discussions

Selection of disaccharide isomers

Ten disaccharide isomers (Figure 1) were chosen with an emphasis on composition isomers, which are epimers that differ by a single subunit. Such isomers generally have more

closely related collision cross sections than connectivity and configuration isomers because their structures differ by only the axial or equitorial position of a single hydroxyl group (e.g. epimers **1** and **2**). In Figure 1a, the six disaccharide isomers (**1**–**6**) correspond to three pairs of composition isomers that differ by a single monosaccharide subunit (epimer pairs **1**/**2**, **3**/**4** and **5**/**6**), two pairs of configuration isomers (α or β anomers, **1**/**3** and **2**/**4**) and two pairs of connectivity (glycosidic linkage) isomers (**3**/**5** and **4**/**6**). Four additional disaccharides (**7**-**10**) were chosen to provide six additional prototypical examples of compositional isomer pairs (epimers **4**/**7**, **3**/**8**, **9**/**10**, **7**/**8**, **3**/**9** and **8**/**10**; Figure 1b). In Figure 1b, all adjacent isomers differ by only the axial or equatorial position of a single hydroxyl group (epimers). Overall, these ten disaccharides correspond to a total of nine pairs of epimers.

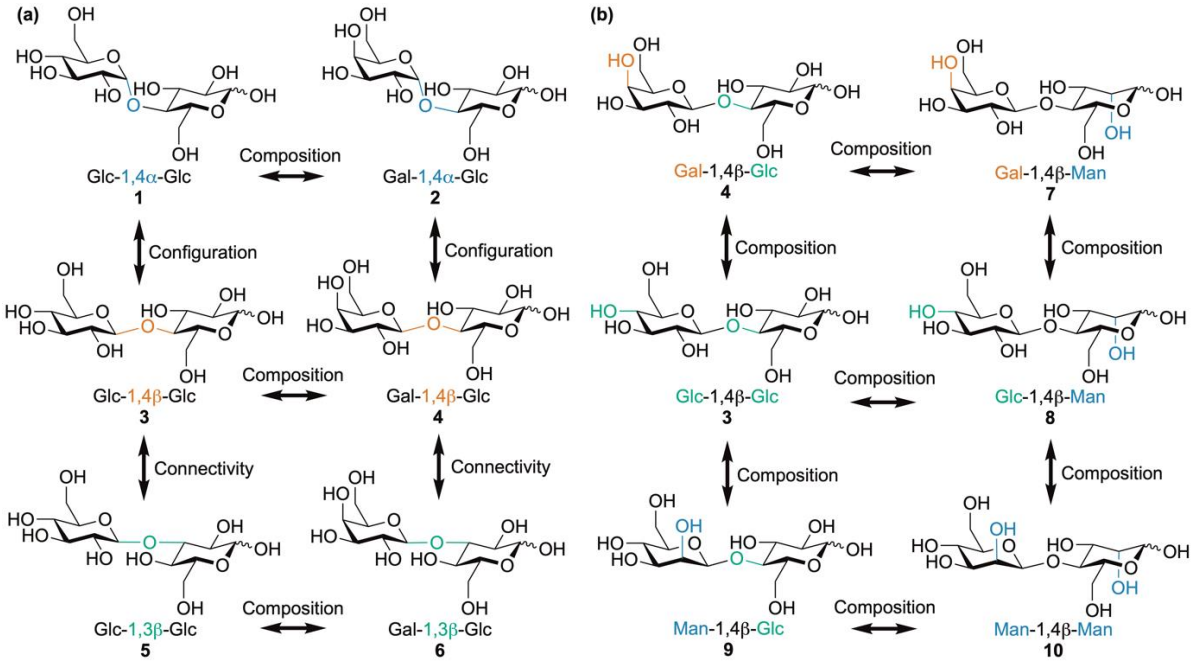

Figure 1. (a) Six of the ten disaccharide isomers investigated here (**1**–**6**). Composition (monosaccharide subunits), configuration (α/β anomers) and connectivity (glycosidic linkage) isomers are indicated by arrows. (b) Six of the ten disaccharides that were investigated are composition isomers (**3**–**4**, **7**–**8**).

Sodiated disaccharide dimer formation and dissociation

ESI-MS and ESI-DMS-MS spectra of 1 mM 4-O-β-D-glucopyranosyl-D-glucose in a 90:10 %(v/v) methanol:water solution containing 1 mM NaCl are shown in Figures S2a and

S2b, respectively. Relatively high concentrations were used to facilitate the formation of non-covalently bound ionic complexes, which can potentially be used to enhance ion separations in DMS. The ions were transmitted through the DMS device in 'transparency mode' with a carrier gas flow rate of 2 L/min (i.e., RF and DC potentials were not applied to the DMS electrodes). In Figures S2a and S2b, the most abundant ion corresponds to the sodiated monomer (*m*/*z* 365). A second ion formed in lower abundance (10%) is assigned to the sodiated dimer (*m*/*z* 707). For each disaccharide, CID of the ion at *m*/*z* 707 resulted in the formation of a major ion at *m*/*z* 365, which is consistent with the precursor ion being assigned to the non-covalently bound sodiated dimer (*e.g.* Figure S2c). Thus, DMS-MS signals corresponding to *m*/*z* 365 can arise both from: (i) the transmission of the sodiated monomer through the DMS device and (ii) higher ionic oligomers that are separated by DMS and then dissociate in the ion source to form the sodiated monomer, which is consistent with previously reported DMS-MS data for lithiated hexose ions.[60]

Optimization

The effects of the temperature, composition, and flow rate of the carrier gas on the DMS resolving power (R_{DMS}) was investigated. R_{DMS} is defined as $\frac{v_C}{w_{1/2}}$, where v_c is the compensation voltage (or compensation field) and $w_{1/2}$ is the full-width half maximum of ion peak. In principle, an increase in the difference between the high and low field mobility should result in an increase in resolving power, which can be obtained by using lower molecular weight carrier gases (e.g. helium).[57, 58] The use of a DMS carrier gas with helium fractions higher than ~50% in N_2(g) resulted in the electrical breakdown of gas within the interelectrode gap[57, 58] and thus, were not used. The use of lower carrier gas flow rates should also increase the resolving power with a corresponding increase in the ion residence time within the interelectrode gap, although at the expense of ion transmission efficiency. By controlling the temperature of the

carrier gas, the signal stability was expected to improve, particularly for Type-C ions that are highly sensitive to ion-neutral clustering during the low-field portion of the waveform.

For all 10 compounds, as the fraction of helium in the carrier gas increased, the peaks generally narrowed (reducing $w_{1/2}$) and the peak centroids shifted to more positive values, resulting in an increase in R_{DMS} for all 10 disaccharides (Figure 2). This observation is in line with the previous studies, which showed that the use of a low molecular weight gas in the carrier gas mixture can significantly improve the separation of ions because of the relatively higher mobility of ions in such gases.[57, 61-63]

In Figure S3, DMS-MS spectra of sodiated disaccharide **4** as a function of the temperature applied to the carrier gas (1:1 He:N_2 with total flow rate of 2 L/min) are shown. Across all temperatures, at least four peaks or partially resolved peaks are observed. As the temperature increases, the spectra change considerably. For example, at 40°C, there are three peaks observed between 32 and 64 V/cm for the sodiated monomer, including a moderately abundant peak at a relatively low compensation field of 32-43 V/cm and a second major peak at around 55 V/cm. With increasing temperature, lower-field peak completely disappears by 100°C which may be attributable to reduced clustering in the low-field portion of the asymmetric AC field. Overall, the DMS spectra are highly sensitive to the temperature of the carrier gas within the analytical gap, which is far lower than the applied temperature (Figure S1).

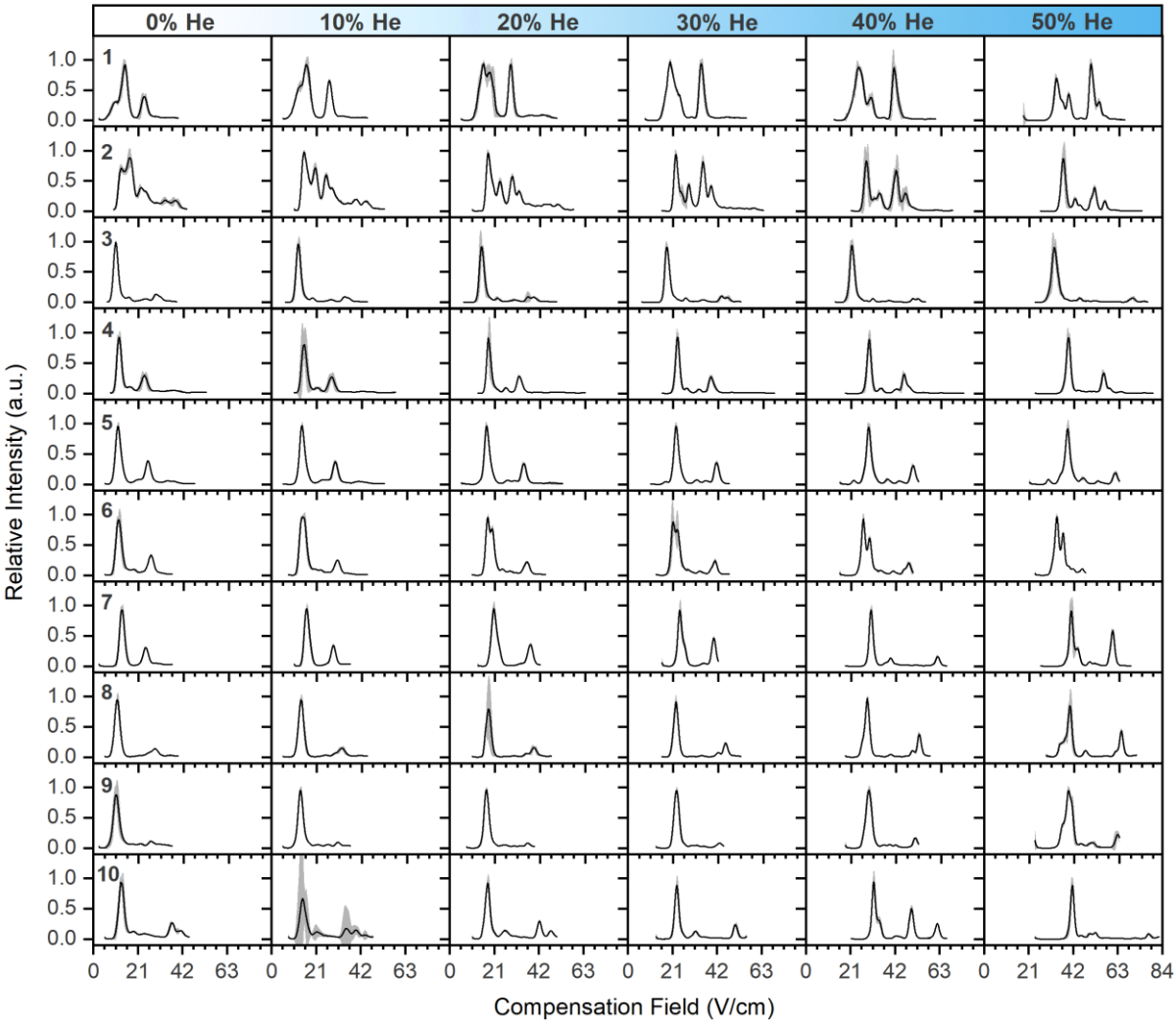

Figure 2. DMS-MS spectra of the sodiated disaccharides $[M+Na]^+$ **1-10** (365 *m/z*) obtained using increasing amounts of helium in the carrier gas (2 L/min). The dispersion field was 22.3 ± 0.1 kV/cm. Data correspond to the mean of four replicates, and the shaded envelopes indicate the error range (95% confidence interval). The carrier gas was not heated.

To further investigate whether the monomer signal can arise from dissociation of the dimer after DMS separation but prior to detection by MS, the monomer spectra were compared to the dimer spectra as a function of the temperature applied to the carrier gas (Figure S3). For a given temperature, the spectra for the monomer and dimer were remarkably similar in terms of the centroids and relative abundances with some key exceptions. In the dimer spectra, the corresponding peak at 32-43 V/cm was absent at all temperatures, unlike in the monomer spectra at lower temperatures. Thus, this lower field peak can be attributed to the transmitted monomer $[M+Na]^+$, whereas the higher field peak cluster is likely the monomer formed by in-

source dissociation of different dimer conformations $[2M+Na]^+$. Furthermore, there is a minor peak near 50 V/cm in the dimer spectra at relatively low temperature that becomes more abundant with increasing temperature (Figure S3). In the monomer spectra, a peak at ~50 V/cm also emerges at ~80-100°C and becomes abundant at higher temperatures (Figure S3), indicating that this peak likely originates from transmission of the sodiated dimer through the DMS electrodes, and then dissociation of the dimer into the sodiated monomer prior to detection. Furthermore, lowering the carrier gas flow rate improved R_{DMS} by 53 to 100% despite signal losses of approximately 98% (Figure S4). The reduction of the longitudinal carrier gas flow velocity between the electrodes increases the ion residence time in the DMS channel and the extent of ion dispersion in the direction perpendicular to the DMS electrodes, enhancing resolution. Such ion dispersion can result in higher ion losses at the narrow capillary inlet to the mass spectrometer.[64]

Overall, the combination of using lower gas flow rates with a higher fraction of He can significantly enhance the resolving power by transmitting ions at higher compensation fields, narrowing the range of compensation fields that ions of a given conformation are transmitted, and 'splitting' broader peaks into several narrower, resolved peaks. For example, in the spectra of 4-O-β-D-glucopyranosyl-D-glucose (monomer), four relatively abundant peaks were measured between 48 and 74 V/cm using 50% He and a flow rate of 1 L/min (Figure S5), which had R_{DMS} values up to 56. In contrast, using 0% He and a flow rate of 2 L/min resulted in the identification of only a single major peak at ~11 V/cm with an R_{DMS} value of ~14 (Figure S5). For 2 L/min flow rates, increasing the extent of He in the carrier gas from 0 to 50% shifted the peak at ~11 V/cm to ~32 V/cm (Figure 2). Owing to the reduced transmission efficiency at lower flow rates, this species became less abundant and was not observed using flow rates as low as 1 L/min (50% He; Figure S6). A lower dispersion field of 21.3 kV was used to ensure that the higher field peak *b* corresponding to the dimer ion that is transmitted through the DMS

electrodes prior to dissociating into monomer (Figure S6) can be detected under these conditions compared to the use of higher dispersion fields (Figure 2). As the carrier gas flow rate is further decreased (50% He), the *b* peak splits into five features (Figure S6). Overall, the R_{DMS} can be enhanced by up to a factor of 14-fold by using low carrier gas flow rates with a high fraction of He (Figure S5).

DMS-MS spectra of disaccharide isomers

Next, the ten disaccharide isomers were analysed by DMS-MS using the optimised separation conditions (i.e. carrier gas at 1 L/min of 50:50% N_2:He, and an applied temperature of 150°C). For clarity, the DMS spectra for all nine compositional isomer pairs (epimers) and the two pairs of both configuration and connectivity isomers are shown in Figures 3 and 4, respectively, with expanded *x*-axis ranges. Overall, multiple DMS-MS peaks were observed between 40-83 V/cm for all disaccharide isomers. In each case, composition, configuration, and connectivity isomers exhibited unique DMS-MS peak patterns in terms of the number of peaks, peak centroids and abundances (Figures 3 and 4). In Table S3, a summary of the peak patterns (peak centroids, widths, and abundances) obtained from Gaussian fitting of clearly resolved peaks is shown. The detection of up to 10 fully and partially resolved peaks for a single analyte (*i.e.* **10**) is distinctive, and not generally observed in the case of low-field IMS or other DMS methods for small ionized molecules,[32, 33] thus enabling the potential identification of different isomers by using a 'fingerprint' approach.

The DMS-MS spectrum for each compositional isomer has one or multiple distinctive peaks and thus, can in principle be fully or partially resolved from its isomer pair (Figure 3 and Table S3). As an example, chosen at random, five peaks were measured for isomer **3** between 48.8 and 73.1 V/cm whereas only two peaks were measured for isomer **4** at 53.7 and 56.6 V/cm, which corresponds to the baseline separation of multiple peaks between the two isomers. In some cases, partial resolution of epimers can be possible. For example, isomer **1** had three

clearly resolved peaks at 49.8, 51.3 and 53.7 V/cm, unlike isomer **2** that also had three peaks but at different compensation fields (48.9, 50.4 and 55.1 V/cm) and relative abundances. As a further example, isomer **9** has two well-resolved peaks at 49.3 and 60.2 V/cm whereas the spectrum of its epimer **10** had three well-resolved, highly abundant peaks at 40.1, 45.4 and 51.6 V/cm. In contrast, isomer **8** has two major peaks at 47.6 and 64.1 V/cm with a shoulder peak at 62.2 V/cm, which should thus enable the differentiation of **8** from its epimer **10** based on the DMS-MS spectra. Overall, the position of a single hydroxyl group (equatorial vs axial) can dramatically impact the DMS spectra of these ions under these conditions.

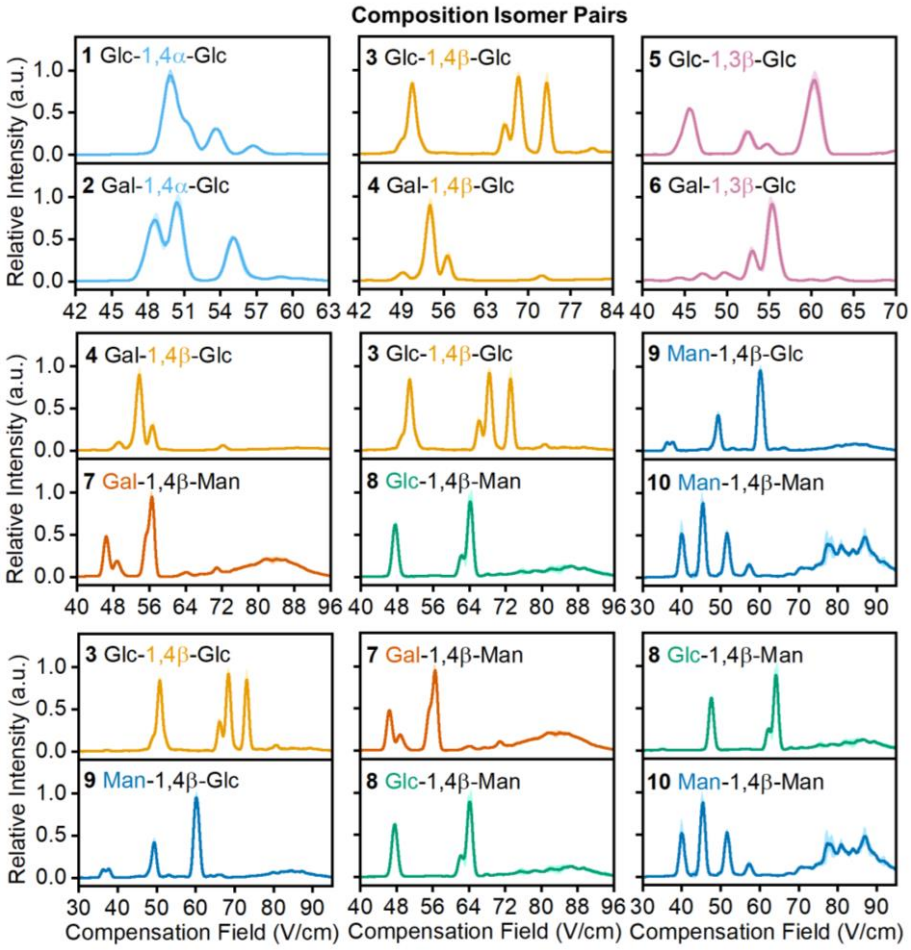

Figure 3. DMS-MS spectra of sodiated monomers $[M+Na]^+$ for composition isomer pairs (epimers). A carrier gas flow rate and temperature of 1 L/min (1:1 He:N_2) and 150°C V were used. The dispersion field was 22.3 ± 0.1 kV/cm.

Like the compositional isomers, each of the configuration and connectivity pairs have multiple distinctive multi-peak patterns including at least one peak that can be resolved either

fully or partially from its isomer pair (Figure 4). For the anomeric pair **1/3**, isomer **3** has three DMS peaks between 66.1 and 73.1 V/cm whereas isomer **1** had essentially no ion signal across this range of compensation fields, and three major peaks between 49.9 and 53.7 V/cm. For the connectivity pair **3**/**5**, isomer **5** had four major peaks between 45.5 and 60.3 V/cm compared to the spectrum for **3** which had three well resolved peaks from 66.1 to 73.1 V/cm.

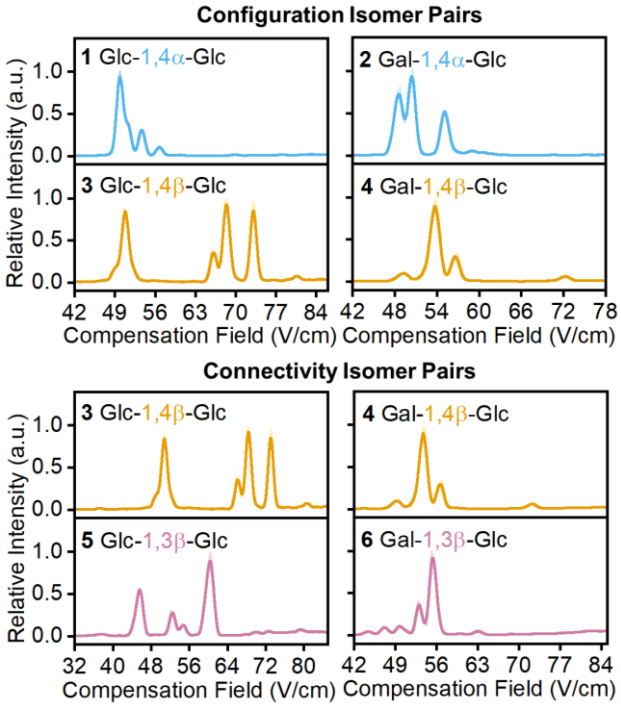

Figure 4. DMS-MS spectra of sodiated monomers $[M+Na]^+$ for configuration (anomers) and connectivity isomer pairs. A carrier gas flow rate and temperature of 1 L/min (1:1 He:N_2) and 150°C V were used. The dispersion field was 22.3 ± 0.1 kV/cm.

By comparing the monomer and dimer DMS-MS spectra (Figure S7) for a given composition isomer, the number of peaks and peak centroids were broadly similar for both monomer and corresponding dimer spectra, but with some exceptions. For example, the number of peaks and corresponding compensation fields of the monomer and dimer spectra of configuration and connectivity isomers (Figure S8) were comparable for **2**, **3** and **4**. However, there were some major differences between the monomer and dimer spectra in some cases. For example, one additional peak for each of isomers **1** and **5** was observed in their dimer spectra compared to the corresponding monomer spectra. For isomers **2** and **6**, the dimer spectra had

two additional major peaks compared to the monomer spectra. Overall, the dimer spectra had the same or more peaks than the monomer spectra. Thus, both the monomer and dimer DMS-MS spectra can potentially be used to differentiate isomers. The use of larger oligomeric cluster ions would likely result in even more complex isomer DMS patterns.

The observation of several or more peaks in ion-mobility spectra has been previously reported for planar macroscale DMS-based analysis of moderately to relatively small ions such as glycopeptides[59] and amino acid complexes.[57, 58] The origin of the multiple peaks in such spectra can be attributed to the presence of multiple conformers including charge solvation isomers during the separation process, in addition to the transmission of dimers and other higher order non-covalent oligomers through the DMS electrodes prior to in-source dissociation. For example, planar macroscale DMS-MS analysis of the proton-bound dimer of tryptophan and N-tert-butoxycarbonyl-O-benzyl-l-serine using 50% He and ~22 kV/cm dispersion field resulted in three major peaks in the spectra, indicating the presence of different proton bound conformers including possible protonation isomers.[57] DMS-MS analysis of T9α-GalNAc glycopeptide isomer using 50% He and ~27 kV/cm dispersion field resulted in the isomers having two distinctive peaks, corresponding to major and minor conformers.[59] For type-C ions, such as those reported here, ion-neutral clustering in the low field portion of the waveform is particularly important and should be highly sensitive to conformation, including the local structure near the charge site. The relatively large number of hydroxyl groups on the carbohydrate ring function as charge acceptor sites for cation adduction, or the formation of transient neutral adducts.[60] Additionally, the disaccharides are conformationally flexible and can readily adopt subtly different conformations, and the O-atoms can likely coordinate the sodium ion in many ways that are energetically competitive. The number of such conformations should increase significantly for dimers and other higher order oligomers. In some cases, the impact of the position of a single hydroxyl group can dramatically affect the

number of DMS species that are resolved (*e.g.* isomers **8** and **10** in Figure 3). Enantiomeric configurations are known to strongly impact the extent of non-covalent clustering in the gas phase. For example, the serine octomer is considered a 'magic' cluster that is preferentially formed in higher abundance for the L-form than the D-form.[65, 66] Furthermore, 'glycans' as small as disaccharides have hydroxyl groups that may align clockwise or counterclockwise with each 6-membered monosaccharide ring, which are connected by a rotatable glycosidic bond. Thus, the ring structures may adopt one of many conformations, in addition to rotatable bonds around C6, and an anomeric carbon at the end of the glycan sequence.[67]

To investigate the effects of lower concentrations, DMS-MS spectra of 4-O-β-D-galactopyranosyl-D-glucose at 20 µM was obtained (Figure S9). Two major DMS peaks were observed, which may be assigned to α and β anomers resulting from mutarotation about the C-1 OH bond.[34] In comparison with the DMS-MS spectrum obtained at higher concentration, both spectra had a major, most abundant peak at ~38 V/cm. However, in the higher concentration spectra, there were more peaks (Figure S9). For example, the abundant peak at 56 V/cm in the higher concentration spectrum is mostly absent at 20 µM, consistent with this peak being assigned to a higher ionic oligomeric peak that is transmitted through the DMS device but subsequently dissociated to a monomer ion in the source. The spectra of the lower concentration solution had a peak at ~73 V/cm with a higher relative intensity than that in the high concentration spectrum, presumably owing to the differential ion clustering potential of α and β anomers.

Next, the separation performance of DMS for a mixture of disaccharide epimers was investigated. In Figures 5a-c, the DMS-MS spectra of the sodiated monomers $[M+Na]^+$ for the composition isomers 4-O-α-D-glucopyranosyl-D-glucose (20 µm) and 4-O-(α-D-galactopyranosyl)-D-glucose (20 µm) that were obtained separately are shown, along with that for the mixture containing both isomers. Both two isomers were separated by > 3 V/cm within

the mixture at a concentration of 20 µm. Similarly, composition isomers 4-O-β-D-glucopyranosyl-D-glucose (20 µm) and 4-O-β-D-galactopyranosyl-D-glucose (20 µm) were also separated by ~ 4 V/cm (Figures 5d-f), indicating that mixtures of epimers at relatively low concentrations can be separated by DMS.

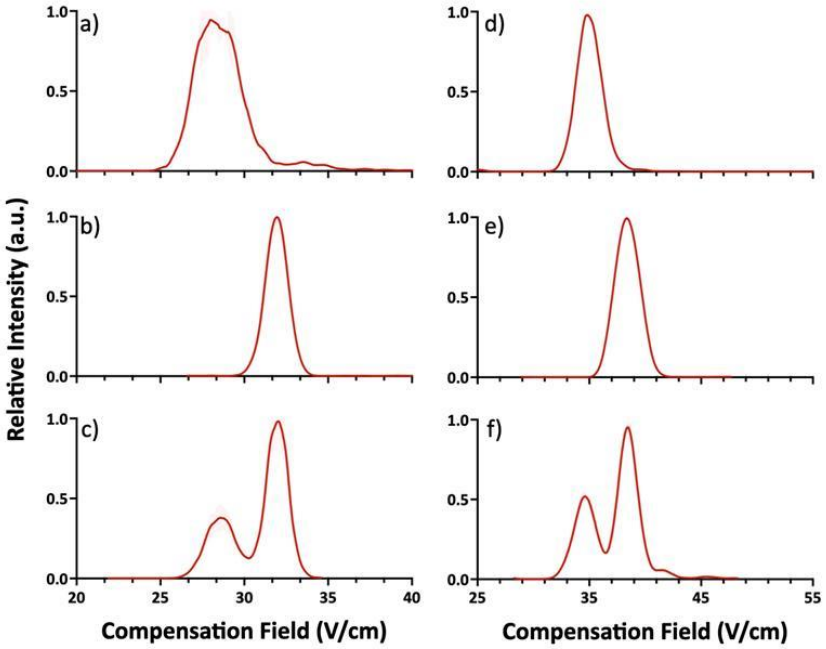

Figure 5. DMS-MS spectra of sodiated monomers $[M+Na]^+$ of the composition epimers (a) 4-O-α-D-glucopyranosyl-D-glucose (**1**), (b) 4-O-(α-D-galactopyranosyl)-D-glucose (**2**), (c) mixture of **1** and **2**, (d) 4-O-β-D-glucopyranosyl-D-glucose (**3**), (e) 4-O-β-D-galactopyranosyl-D-glucose (**4**), and (f) a mixture of **3** and **4**. A carrier gas flow rate of 2 L/min (1:1 He:N_2) at ambient temperature was used. The dispersion field was 21.3 ± 0.1 kV/cm.

Conclusions

In this study, the separation and detection of a range of epimeric, connectivity and anomeric disaccharide isomers using high-resolution differential ion mobility-mass spectrometry (DMS-MS) is demonstrated. By use of an 'optimal' carrier gas composition and flow rate, and temperature, the resolving power of DMS was increased up-to 14-fold, and nine composition (monosaccharide subunits), two configuration (α/β anomers) and two connectivity (glycosidic linkage) isomer pairs could be reproducibly differentiated. At low concentrations, DMS-MS was able to readily separate disaccharide epimers in simple mixtures. At high concentrations, DMS-MS spectra of different disaccharides exhibited complex, multi-peak

spectra with a single disaccharide resulting in up-to ten peaks. Remarkably, the difference in the axial or equatorial position of a single hydroxyl group (*i.e.* in epimeric pairs) can dramatically affect the resulting DMS-MS spectral profiles. The complexity of peak distributions in the DMS-MS spectra also opens the possibility for identification based on database searching. A holistic "fingerprint" analysis could be used to determine unknown compounds through automated spectral matching and/or manual 'lookup' tables (*e.g.* Table S3). It is anticipated that the incorporation of DMS with complementary ion mobility and MS-based glycomics and glycoproteomic instrumental platforms can potentially be used to enhance the characterization of more complex glycans and glycoconjugates. For instance, DMS can be used to selectively introduce a given ion conformation into a low-field IMS instrument in a separation process that takes milliseconds. Thus, the integration of DMS with advanced MS-based methods is anticipated to enhance the characterisation of glycans.

Acknowledgments

The authors acknowledge Dr Ezaz Ahmed for collecting some of the ESI-MS data. KMMK and WAD acknowledge funding from Australian Research Council (DE190100986 and FT200100798, respectively).

Author Information

KMMK: orcid.org/0000-0003-3742-5742

WAD: orcid.org/0000-0002-6622-8193

XH: orcid.org/0000-0003-2681-0370

References

1. Karczewski, K. J.; Snyder, M. P., Integrative omics for health and disease. *Nature Reviews Genetics* **2018,** *19*, 299-310.

2. Green, E. D.; Guyer, M. S., Charting a course for genomic medicine from base pairs to bedside. *Nature* **2011,** *470*, 204-213.

3. Cummings, R. D.; Pierce, J. M., The challenge and promise of glycomics. *Chemistry & Biology* **2014,** *21*, 1-15.

4. McNaught, A. D.; Wilkinson, A., *Compendium of Chemical Terminology*. Blackwell Science Oxford: 1997; Vol. 1669.

5. Varki, A.; Cummings, R. D.; Aebi, M.; Packer, N. H.; Seeberger, P. H.; Esko, J. D.; Stanley, P.; Hart, G.; Darvill, A.; Kinoshita, T., Symbol nomenclature for graphical representations of glycans. *Glycobiology* **2015,** *25*, 1323-1324.

6. Wopereis, S.; Lefeber, D. J.; Morava, E.; Wevers, R. A., Mechanisms in protein O-glycan biosynthesis and clinical and molecular aspects of protein O-glycan biosynthesis defects: a review. *Clinical Chemistry* **2006,** *52*, 574-600.

7. Dove, A., The bittersweet promise of glycobiology. *Nature Biotechnology* **2001,** *19*, 913-917.

8. De Reggi, M.; Capon, C.; Gharib, B.; Wieruszeski, J. M.; Michel, R.; Fournet, B., The glycan moiety of human pancreatic lithostathine: structure characterization and possible pathophysiological implications. *European Journal of Biochemistry* **1995,** *230*, 503-510.

9. Rudd, P. M.; Mattu, T. S.; Zitzmann, N.; Mehta, A.; Colominas, C.; Hart, E.; Opdenakker, G.; Dwek, R. A., Glycoproteins: rapid sequencing technology for N-linked and GPI anchor glycans. *Biotechnology and Genetic Engineering Reviews* **1999,** *16*, 1-22.

10. Schedin-Weiss, S.; Winblad, B.; Tjernberg, L. O., The role of protein glycosylation in Alzheimer disease. *The FEBS Journal* **2014,** *281*, 46-62.

11. Merrill Jr, A.; Vu, M., Glycolipids. **2016**.

12. Ashline, D. J.; Lapadula, A. J.; Liu, Y.-H.; Lin, M.; Grace, M.; Pramanik, B.; Reinhold, V. N., Carbohydrate structural isomers analyzed by sequential mass spectrometry. *Analytical Chemistry* **2007,** *79*, 3830-3842.

13. Devakumar, A.; Mechref, Y.; Kang, P.; Novotny, M. V.; Reilly, J. P., Identification of isomeric N-glycan structures by mass spectrometry with 157 nm laser-induced photofragmentation. *Journal of The American Society for Mass Spectrometry* **2008,** *19*, 1027-1040.

14. Shi, S. D.-H.; Hendrickson, C. L.; Marshall, A. G.; Siegel, M. M.; Kong, F.; Carter, G. T., Structural validation of saccharomicins by high resolution and high mass accuracy fourier transform-ion cyclotron resonance-mass spectrometry and infrared multiphoton dissociation tandem mass spectrometry. *Journal of The American Society for Mass Spectrometry* **1999,** *10*, 1285-1290.

15. Xie, Y.; Lebrilla, C. B., Infrared multiphoton dissociation of alkali metal-coordinated oligosaccharides. *Analytical Chemistry* **2003,** *75*, 1590-1598.

16. Zhang, J.; Schubothe, K.; Li, B.; Russell, S.; Lebrilla, C. B., Infrared multiphoton dissociation of O-linked mucin-type oligosaccharides. *Analytical Chemistry* **2005,** *77*, 208-214.

17. Lancaster, K. S.; An, H. J.; Li, B.; Lebrilla, C. B., Interrogation of N-linked oligosaccharides using infrared multiphoton dissociation in FT-ICR mass spectrometry. *Analytical Chemistry* **2006,** *78*, 4990-4997.

18. Budnik, B.; Haselmann, K.; Elkin, Y. N.; Gorbach, V.; Zubarev, R., Applications of electron− ion dissociation reactions for analysis of polycationic chitooligosaccharides in Fourier transform mass spectrometry. *Analytical Chemistry* **2003,** *75*, 5994-6001.

19. Adamson, J. T.; Håkansson, K., Electron capture dissociation of oligosaccharides ionized with alkali, alkaline earth, and transition metals. *Analytical Chemistry* **2007,** *79*, 2901-2910.

20. Stephens, E.; Maslen, S. L.; Green, L. G.; Williams, D. H., Fragmentation characteristics of neutral N-linked glycans using a MALDI-TOF/TOF tandem mass spectrometer. *Analytical Chemistry* **2004,** *76*, 2343-2354.

21. Mechref, Y.; Kang, P.; Novotny, M. V., Differentiating structural isomers of sialylated glycans by matrix-assisted laser desorption/ionization time-of-flight/time-of-flight tandem mass spectrometry. *Rapid Communications in Mass Spectrometry* **2006,** *20*, 1381-1389.

22. Spina, E.; Sturiale, L.; Romeo, D.; Impallomeni, G.; Garozzo, D.; Waidelich, D.; Glueckmann, M., New fragmentation mechanisms in matrix-assisted laser desorption/ionization time-of-flight/time-of-flight tandem mass spectrometry of carbohydrates. *Rapid Communications in Mass Spectrometry* **2004,** *18*, 392-398.

23. Morelle, W.; Slomianny, M. C.; Diemer, H.; Schaeffer, C.; Dorsselaer, A. v.; Michalski, J. C., Fragmentation characteristics of permethylated oligosaccharides using a

matrix-assisted laser desorption/ionization two-stage time-of-flight (TOF/TOF) tandem mass spectrometer. *Rapid Communications in Mass Spectrometry* **2004,** *18*, 2637-2649.

24. Zhao, J.; Simeone, D. M.; Heidt, D.; Anderson, M. A.; Lubman, D. M., Comparative serum glycoproteomics using lectin selected sialic acid glycoproteins with mass spectrometric analysis: application to pancreatic cancer serum. *Journal of Proteome Research* **2006,** *5*, 1792-1802.

25. Ruhaak, L. R.; Miyamoto, S.; Kelly, K.; Lebrilla, C. B., N-Glycan profiling of dried blood spots. *Analytical Chemistry* **2012,** *84*, 396-402.

26. Chu, C. S.; Niñonuevo, M. R.; Clowers, B. H.; Perkins, P. D.; An, H. J.; Yin, H.; Killeen, K.; Miyamoto, S.; Grimm, R.; Lebrilla, C. B., Profile of native N-linked glycan structures from human serum using high performance liquid chromatography on a microfluidic chip and time-of-flight mass spectrometry. *Proteomics* **2009,** *9*, 1939-1951.

27. Hua, S.; An, H. J.; Ozcan, S.; Ro, G. S.; Soares, S.; DeVere-White, R.; Lebrilla, C. B., Comprehensive native glycan profiling with isomer separation and quantitation for the discovery of cancer biomarkers. *Analyst* **2011,** *136*, 3663-3671.

28. Kammeijer, G. S.; Jansen, B. C.; Kohler, I.; Heemskerk, A. A.; Mayboroda, O. A.; Hensbergen, P. J.; Schappler, J.; Wuhrer, M., Sialic acid linkage differentiation of glycopeptides using capillary electrophoresis–electrospray ionization–mass spectrometry. *Scientific Reports* **2017,** *7*, 1-10.

29. Shao, L.; Haltiwanger, R., O-fucose modifications of epidermal growth factor-like repeats and thrombospondin type 1 repeats: unusual modifications in unusual places. *Cellular and Molecular Life Sciences* **2003,** *60*, 241-250.

30. Morrison, K. A.; Clowers, B. H., Contemporary glycomic approaches using ion mobility–mass spectrometry. *Current Opinion in Chemical Biology* **2018,** *42*, 119-129.

31. Fenn, L. S.; McLean, J. A., Structural separations by ion mobility-MS for glycomics and glycoproteomics. In *Mass Spectrometry of Glycoproteins*, Springer: 2013; pp 171-194.

32. Hofmann, J.; Pagel, K., Glycan analysis by ion mobility–mass spectrometry. *Angewandte Chemie International Edition* **2017,** *56*, 8342-8349.

33. Hofmann, J.; Hahm, H.; Seeberger, P. H.; Pagel, K., Identification of carbohydrate anomers using ion mobility–mass spectrometry. *Nature* **2015,** *526*, 241-244.

34. Nagy, G.; Attah, I. K.; Garimella, S. V. B.; Tang, K.; Ibrahim, Y. M.; Baker, E. S.; Smith, R. D., Unraveling the isomeric heterogeneity of glycans: ion mobility separations in structures for lossless ion manipulations. *Chemical Communications* **2018,** *54*, 11701-11704.

35. Sastre Toraño, J.; Aizpurua-Olaizola, O.; Wei, N.; Li, T.; Unione, L.; Jiménez-Osés, G.; Corzana, F.; Somovilla, V. J.; Falcon-Perez, J. M.; Boons, G.-J., Identification of Isomeric N-Glycans by Conformer Distribution Fingerprinting using Ion Mobility Mass Spectrometry. *Chemistry – A European Journal* **2021,** *27*, 2149-2154.
36. Yang, H.; Shi, L.; Zhuang, X.; Su, R.; Wan, D.; Song, F.; Li, J.; Liu, S., Identification of structurally closely related monosaccharide and disaccharide isomers by PMP labeling in conjunction with IM-MS/MS. *Scientific Reports* **2016,** *6*, 1-9.
37. Williamson, D. L.; Bergman, A. E.; Nagy, G., Investigating the Structure of α/β Carbohydrate Linkage Isomers as a Function of Group I Metal Adduction and Degree of Polymerization as Revealed by Cyclic Ion Mobility Separations. *Journal of the American Society for Mass Spectrometry* **2021,** *32*, 2573-2582.
38. Ujma, J.; Ropartz, D.; Giles, K.; Richardson, K.; Langridge, D.; Wildgoose, J.; Green, M.; Pringle, S., Cyclic Ion Mobility Mass Spectrometry Distinguishes Anomers and Open-Ring Forms of Pentasaccharides. *Journal of The American Society for Mass Spectrometry* **2019,** *30*, 1028-1037.
39. Ben Faleh, A.; Warnke, S.; Rizzo, T. R., Combining ultrahigh-resolution ion-mobility spectrometry with cryogenic infrared spectroscopy for the analysis of glycan mixtures. *Analytical Chemistry* **2019,** *91*, 4876-4882.
40. Warnke, S.; Ben Faleh, A.; Scutelnic, V.; Rizzo, T. R., Separation and Identification of Glycan Anomers Using Ultrahigh-Resolution Ion-Mobility Spectrometry and Cryogenic Ion Spectroscopy. *Journal of The American Society for Mass Spectrometry* **2019,** *30*, 2204-2211.
41. Bansal, P.; Yatsyna, V.; AbiKhodr, A. H.; Warnke, S.; Ben Faleh, A.; Yalovenko, N.; Wysocki, V. H.; Rizzo, T. R., Using SLIM-Based IMS-IMS Together with Cryogenic Infrared Spectroscopy for Glycan Analysis. *Analytical Chemistry* **2020,** *92*, 9079-9085.
42. Gabryelski, W.; Froese, K. L., Rapid and sensitive differentiation of anomers, linkage, and position isomers of disaccharides using high-field asymmetric waveform ion mobility spectrometry (FAIMS). *Journal of The American Society for Mass Spectrometry* **2003,** *14*, 265-277.
43. Levin, D. S.; Vouros, P.; Miller, R. A.; Nazarov, E. G., Using a nanoelectrospray-differential mobility spectrometer-mass spectrometer system for the analysis of oligosaccharides with solvent selected control over ESI aggregate ion formation. *Journal of The American Society for Mass Spectrometry* **2007,** *18*, 502-511.

44. Lane, C. S.; McManus, K.; Widdowson, P.; Flowers, S. A.; Powell, G.; Anderson, I.; Campbell, J. L., Separation of sialylated glycan isomers by differential mobility spectrometry. *Analytical Chemistry* **2019,** *91*, 9916-9924.

45. Creese, A. J.; Cooper, H. J., Separation and identification of isomeric glycopeptides by high field asymmetric waveform ion mobility spectrometry. *Analytical Chemistry* **2012,** *84*, 2597-2601.

46. Kabir, K. M. M.; Donald, W. A., Microscale differential ion mobility spectrometry for field deployable chemical analysis. *Trends in Analytical Chemistry* **2017,** *97*, 399-427.

47. Winter, D. L.; Wilkins, M. R.; Donald, W. A., Differential Ion Mobility–Mass Spectrometry for Detailed Analysis of the Proteome. *Trends in Biotechnology* **2019,** *37*, 198-213.

48. Shvartsburg, A. A.; Creese, A. J.; Smith, R. D.; Cooper, H. J., Separation of peptide isomers with variant modified sites by high-resolution differential ion mobility spectrometry. *Analytical Chemistry* **2010,** *82*, 8327-8334.

49. Shvartsburg, A. A.; Singer, D.; Smith, R. D.; Hoffmann, R., Ion mobility separation of isomeric phosphopeptides from a protein with variant modification of adjacent residues. *Analytical Chemistry* **2011,** *83*, 5078-5085.

50. Shvartsburg, A. A.; Zheng, Y.; Smith, R. D.; Kelleher, N. L., Separation of variant methylated histone tails by differential ion mobility. *Analytical chemistry* **2012,** *84*, 6317-6320.

51. Shvartsburg, A. A.; Li, F.; Tang, K.; Smith, R. D., High-Resolution Field Asymmetric Waveform Ion Mobility Spectrometry Using New Planar Geometry Analyzers. *Analytical Chemistry* **2006,** *78*, 3706-3714.

52. Shvartsburg, A. A.; Tang, K.; Smith, R. D., Modeling the resolution and sensitivity of FAIMS analyses. *Journal of the American Society for Mass Spectrometry* **2004,** *15*, 1487-1498.

53. Campbell, J. L.; Kafle, A.; Bowman, Z.; Blanc, J. C. Y. L.; Liu, C.; Hopkins, W. S., Separating chiral isomers of amphetamine and methamphetamine using chemical derivatization and differential mobility spectrometry. *Anal. Sci. Adv.* **2020,** *1*, 233-244.

54. Anwar, A.; Psutka, J.; Walker, S. W. C.; Dieckmann, T.; Janizewski, J. S.; Larry Campbell, J.; Scott Hopkins, W., Separating and probing tautomers of protonated nucleobases using differential mobility spectrometry. *International Journal of Mass Spectrometry* **2018,** *429*, 174-181.

55. Winter, D. L.; Mastellone, J.; Kabir, K. M. M.; Wilkins, M. R.; Donald, W. A., Separation of Isobaric Mono- and Dimethylated RGG-Repeat Peptides by Differential Ion Mobility-Mass Spectrometry. *Analytical Chemistry* **2019,** *91*, 11827-11833.
56. Zhang, J. D.; Donor, M. T.; Rolland, A. D.; Leeming, M. G.; Wang, H.; Trevitt, A. J.; Kabir, K. M. M.; Prell, J. S.; Donald, W. A., Protonation isomers of highly charged protein ions can be separated in FAIMS-MS. *International Journal of Mass Spectrometry* **2020,** *457*, 116425.
57. Zhang, J. D.; Kabir, K. M. M.; Lee, H. E.; Donald, W. A., Chiral recognition of amino acid enantiomers using high-definition differential ion mobility mass spectrometry. *International Journal of Mass Spectrometry* **2018,** *428*, 1-7.
58. Zhang, J. D.; Kabir, K. M. M.; Donald, W. A., Chapter Three - Ion-Mobility Mass Spectrometry for Chiral Analysis of Small Molecules. In *Comprehensive Analytical Chemistry*, Donald, W. A.; Prell, J. S., Eds. Elsevier: 2019; Vol. 83, pp 51-81.
59. Pathak, P.; Baird, M. A.; Shvartsburg, A. A., High-Resolution Ion Mobility Separations of Isomeric Glycoforms with Variations on the Peptide and Glycan Levels. *J. Am. Soc. Mass Spectrom.* **2020,** *31*, 1603-1609.
60. Campbell, M. T.; Chen, D.; Wallbillich, N. J.; Glish, G. L., Distinguishing Biologically Relevant Hexoses by Water Adduction to the Lithium-Cationized Molecule. *Analytical Chemistry* **2017,** *89*, 10504-10510.
61. Zhang, J. D.; Kabir, K. M. M.; Donald, W. A., Metal-ion free chiral analysis of amino acids as small as proline using high-definition differential ion mobility mass spectrometry. *Analytica Chimica Acta* **2018,** *1036*, 172-178.
62. Shvartsburg, A. A.; Seim, T. A.; Danielson, W. F.; Norheim, R.; Moore, R. J.; Anderson, G. A.; Smith, R. D., High-definition differential ion mobility spectrometry with resolving power up to 500. *Journal of the American Society for Mass Spectrometry* **2013,** *24*, 109-114.
63. Shvartsburg, A. A.; Ibrahim, Y. M.; Smith, R. D., Differential ion mobility separations in up to 100% helium using microchips. *Journal of the American Society for Mass Spectrometry* **2014,** *25*, 480-489.
64. Kabir, K. M. M.; Ahmed, E.; Donald, W. A., An atmospheric pressure ion funnel with a slit entrance for enhancing signal and resolution in high resolution differential ion mobility mass spectrometry. *Analyst* **2022,** *147*, 870-879.

65. Cooks, R. G.; Zhang, D.; Koch, K. J.; Gozzo, F. C.; Eberlin, M. N., Chiroselective Self-Directed Octamerization of Serine: Implications for Homochirogenesis. *Analytical Chemistry* **2001,** *73*, 3646-3655.

66. Schalley, C. A.; Weis, P., Unusually stable magic number clusters of serine with a surprising preference for homochirality. *International Journal of Mass Spectrometry* **2002,** *221*, 9-19.

67. Simons, J. P.; Jockusch, R. A.; ÇarÇabal, P.; Hünig, I.; Kroemer, R. T.; Macleod, N. A.; Snoek, L. C., Sugars in the gas phase. Spectroscopy, conformation, hydration, co-operativity and selectivity. *International Reviews in Physical Chemistry* **2005,** *24*, 489-531.